Journal of Inorganic Biochemistry 201 (2019) 110818

Contents lists available at ScienceDirect

Journal of Inorganic Biochemistry

journal homepage: www.elsevier.com/locate/jinorgbio

BioMOF@cellulose fabric composites for bioactive molecule delivery

Seyyed Abbas Noorian[a,b], Nahid Hemmatinejad[a,*], Jorge A.R. Navarro[b,*]

[a] Textile Engineering Department, Amirkabir University of Technology, Tehran, Iran
[b] Departamento de Química Inorgánica, Universidad de Granada, Av. Fuentenueva, S/N, 18071 Granada, Spain

ARTICLE INFO

Keywords:
Bio metal-organic frameworks (BioMOF)
Cotton fabric
in situ synthesis
Bioactive molecule delivery
Wound dressing

ABSTRACT

This work describes *in situ* synthesis and application of the zinc glutamate Bio Metal-Organic Framework (BioMOF) supported on cellulose fabrics as a dual material for nitric oxide (NO) and 5-fluorouracil (5FU) controlled delivery for wound and/or skin cancer therapy. *In situ* synthesis of BioMOF on the cotton fabric was successfully achieved and the incorporation of NO and 5FU was studied. We have observed that BioMOF doped with Fe^{II} metal ions has a beneficial impact on NO incorporation. The products obtained were analyzed with X-ray powder diffraction (XRPD), Fourier-Transform Infrared Spectroscopy-Attenuated Total Reflectance (FTIR-ATR), Field Emission Scanning Electron Microscopy (FESEM), Diffuse Reflectance UV–Vis-NIR spectrometer, X-Ray pHotoelectron Spectroscopy (XPS), Thermogravimetric Analysis (TGA), N_2 adsorption analysis, Transition UV–Visible spectroscopy, and Gas Chromatography-Mass Spectroscopy (GC–MS). Moreover, antibacterial and anticancer activity in melanoma skin cell was carried out in order to prove the biological activity of the drug-loaded BioMOF on treated cellulose fabrics. These studies are indicative of the potential of BioMOF@cellulose fabric composites for the controlled delivery of bioactive molecules on the wound and/or cancer.

1. Introduction

An increase in the global concern toward the incidence of skin cancer, epidermal damage, such as ulcer, burn, or other traumatic incidents, which have been witnessed in recent years with a concomitant enhanced focus on the development of new therapies [1,2]. Therefore, various modified wound dressings have been developed to promote the skin cancer therapy and wound healing [3]. In particular, materials for the controlled delivery of bioactive molecules were desired for developing antibacterial and anticancer properties on the wound dressings. The high tailorable nature of structure and properties of Metal-Organic Frameworks (MOFs) have gained interest as suitable controlled drug releasing materials [4,5]. MOF materials can be used for the controlled delivery of bioactive agents, depending on the chemical pore nature, their stability, drug-MOF interaction, drug loading capacity, kinetics of release, size distribution, *etc.* [6]. The bioactive agents can range from small gaseous molecules (*e.g.*, nitric oxide, carbon monoxide) coordinated to unsaturated metal centers to small active pharmaceutical molecules (5-fluorouracil [7], caffeine [8], ibuprofen, mitoxantrone [9]) adsorbed in the pore network or bioactive pro-drugs employed as framework linkers [4]. Some of the limitations of this strategy are the possible toxicity of constituent of the MOF systems. These can overcome by the use of naturally occurring organic linkers and metal ions leading to Biomolecule-based Metal-Organic Frameworks (BioMOF) materials [10].

The zinc glutamate is one kind of flexible BioMOF structure with the pore size of 13 Å, in which metal-oxygen and metal-nitrogen bondings are responsible for establishing of a pore structure [11], and numerous types of electrostatic and hydrogen bondings can incorporate bioactive molecules (Fig. 1). Moreover, from the point of cost, availability, biodegradability, biocompatibility and guests loading capability of flexible zinc glutamate BioMOF can be employed for various academic field and industrial applications, especially, health care/medical applications [12].

Commonly, two methods have been reported for loading drug with the MOF such as two-step encapsulation by soaking MOF in saturated drug solution or grinding drug with MOF, and one-pot synthesis and loading method [13]. The one-pot synthesis and loading method would allow systematic loading of the drug on MOF in one step and consequently decreases the time of process and dissipation of materials. Moreover, the constraint in loading drug as a result of microporosity of MOF can overcome by this method. In other words, the one-pot synthesis and loading method provides a more comfortable situation for entering drug molecules into the pores of MOFs [7]. Therefore, the storage and controlled release of drug from MOF are enhanced.

The functionalization of MOF also would allow systematic

* Corresponding authors.
E-mail addresses: hemmati@aut.ac.ir (N. Hemmatinejad), jarn@ugr.es (J.A.R. Navarro).

https://doi.org/10.1016/j.jinorgbio.2019.110818
Received 3 July 2019; Received in revised form 27 August 2019; Accepted 1 September 2019
Available online 05 September 2019
0162-0134/

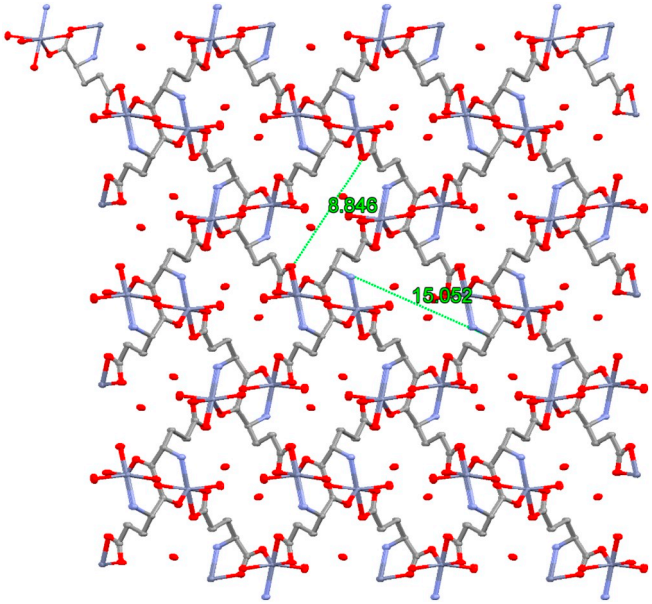

Fig. 1. Coordinated H_2O molecules and H-bonded ones (crystal lattices) in the framework of BioMOF, viewed along c-axis. Packing diagram (a), Legend: gray C-atoms; red O-atoms; Cadet blue Zn-atom; and blue N-atoms. (For interpretation of the references to color in this figure legend, the reader is referred to the web version of this article.)

modification of the structure and enhance the loading efficiency of bioactive molecules and controlled release behavior [14]. The functionalized MOF with unsaturated metal sites such as iron(II) (Fe^{II}) is also highly valuable for the capture and delivery of nitric oxide (NO) gas [15]. NO gas used as antiplatelet activator, antithrombotic, vasodilation, antibacterial and anti-inflammatory agents for localized therapeutics due to the short physiological half-life of NO (0.09 to > 2 s) [16–19]. Therefore, store and controlled release of NO gas are essential for a wide variety of biomedicine applications, especially in skin therapy applications [18–20].

This work is focused on preparation and characterization of Fe^{II} and 5-fluorouracil (5FU) loaded BioMOF using one-pot synthesis and loading method and one step *in situ* synthesis and applying of these materials on the cotton fabric to impart NO and 5FU controlled release properties and therefore antibacterial and anticancer properties for treated cotton fabric. In this respect, the X-ray powder diffraction (XRPD) pattern, chemical interaction (by Fourier-Transform Infrared Spectroscopy-Attenuated Total Reflectance (FTIR-ATR) and X-Ray Photoelectron Spectroscopy (XPS) analyses), size and morphology (by Field Emission Scanning Electron Microscopy (FESEM)), NO and 5FU release behavior (by Gas chromatography-mass spectrometry and UV–visible spectrophotometer), kinetic model of release, antibacterial and *in vitro* anticancer effects were studied.

2. Experimental

2.1. Materials and methods

L-Glutamic acid hydrochloride, zinc chloride, sodium hydroxide, iron(II) perchlorate $Fe(ClO_4)_2$, Dulbecco's Phosphate buffered saline (PBS), modified Griess reagent, and 5-fluorouracil (5FU) were purchased from Sigma Aldrich and used without any additional purification. The cancer cell line B16F10 was supplied by the bank of cells at CIC of the University of Granada (REFERENCE N°: ATCC N°: CRL-6322 (lot CB No)).

Desized and bleached cotton plain-woven fabric (100% cellulose, 117.5 g/m^2), was supplied as cellulosic substrates. Before being used, all the cotton samples were washed by the nonionic surfactant Adrasil HP (P-836, ADRASA, Spain, 1 g/L) at the liquor-to-fabric ratio of 60:1. After 30 min of washing at 50 °C, the fabrics were rinsed for several times with warm and then cold water and dried at the ambient temperature. Before any treatment, the cotton fabrics were treated with an alkaline solution (2 g/L NaOH at 60 °C for 30 min) to promote the active site on the surface of the fabric.

2.1.1. Synthesis of the BioMOF

The synthesis of zinc glutamate BioMOF in microcrystalline powder form was adopted from the previously cited report [12]. Briefly, the BioMOF was prepared by stirring the mixture of L-glutamic acid hydrochloride (6 mmol), NaOH (18 mmol) and $ZnCl_2$ (6 mmol) in 50 ml aqueous solution for 30 min at 100 °C. The readily precipitated white powder was filtered and washed several times with distilled water. Then, pure zinc glutamate BioMOF powder was dried in air at room temperature.

2.1.2. One-pot synthesis of the Fe-BioMOF & 5FU-BioMOF

The Fe-BioMOF or 5FU-BioMOF were one-pot synthesized according to BioMOF preparation process, adding 1.8 mmol $Fe(ClO_4)_2$ or 0.3 mmol 5FU to synthesis solution under an Ar atmosphere. To achieve high loading efficiency, $Fe(ClO_4)_2$: L-glutamic acid hydrochloride: $ZnCl_2$ and 5FU: L-glutamic acid hydrochloride: $ZnCl_2$ were used at the concentration ratios of 0.3:1:1 and 0.05:1:1, respectively. The readily precipitated powder was filtered and washed several times with distilled water. Then, the powder was dried in air at room temperature.

2.1.3. In situ synthesis of the BioMOF on cotton fabric

The BioMOF nanoparticles have been *in situ* synthesized on cotton fabric (BioMOF-Fa) according to BioMOF synthesis (section 2.1.1). In this regards, the alkaline treated cotton fabric was immersed in 0.2 M zinc chloride ($ZnCl_2$) aqueous solution and then L-glutamic acid hydrochloride (0.2 M) aqueous solution was added under vigorous stirring. After that, the pH of the resultant solution is adjusted to 8 by adding 0.6 M NaOH aqueous solution, and the mixture is stirred vigorously for 30 min. After that, the solution was kept stirring at 100 °C for 30 min. Then, the treated cotton fabric was washed by the distilled water and dried at the room temperature.

2.1.4. One step in situ and applying of the Fe-BioMOF & 5FU-BioMOF on cotton fabric

The one-step *in situ* synthesis, loading, and applying of Fe-BioMOF and 5FU-BioMOF nanoparticles on cotton fabric have been performed similarly to the above described BioMOF-Fa method. 0.06 M $Fe(ClO_4)_2$ and 0.01 M 5FU were used as doping agents to achieve Fe-BioMOF-Fa and 5FU-BioMOF-Fa, respectively. Moreover, to determine the effect of 5FU on the pristine cotton fabric, the cotton fabric was treated with the same amount of 5FU according to *in situ* synthesis leading to 5FU-BioMOF preparation method. This cotton fabric named 5FU-Fa in this study.

2.2. Characterization

2.2.1. X-ray powder diffraction analysis

The X-ray powder diffraction (XRPD) patterns of samples were attained by using a Bruker XRPD (D2 PHASER, Germany) diffractometer equipment. Diffraction intensity spectra were collected by scanning in the 2θ range of 5–35° with 0.1° steps by Ni-filtered Cu (Kα = 0.15418 nm) radiation source.

2.2.2. FTIR-attenuated total reflectance analysis

FTIR-ATR of the sample powders and treated cotton fabric were recorded with a diamond PIKE Technology GladiATR mode using a TENSOR 27 FTIR-ATR Spectrometer (Bruker, Germany). For both powder and fabric samples, the FTIR-ATR spectra were studied in the wavenumber range of 4000–400 cm^{-1} with a resolution of 4 cm^{-1}.

2.2.3. Morphology and size study

The morphology and size of BioMOF and BioMOF-Fa were evaluated by High-Resolution Field Emission Scanning Electron Microscopy (FESEM) Zeiss SUPRA40VP instrument. Before FESEM analysis, the samples were covered with a thin gold layer by POLARON E5000. Energy-dispersive X-Ray spectroscopy (EDX) of the powders and fibers was performed by using an X-Max large surface detector 50 mm (Oxford, UK). The ImageJ software was used to study the size distribution by image processing and analysis of FESEM images and the average size of 50 particles were measured.

2.2.4. Diffuse reflectance UVis-NIR spectrophotometer

The diffuse reflectance of Fe-BioMOF was obtained through using Ultraviolet, visible and near-infrared diffusion spectrophotometer (VARIAN mod. Cary-5E) in the range of 200–2000 nm and $BaSO_4$ was used as a reference standard.

2.2.5. X-ray photoelectron spectroscopy

X-ray photoelectron spectroscopy (XPS) measurement was carried out to evaluate the chemistry of powder samples and fabric swatches by using a Kratos Axis Ultra-DLD XPS utilizing an Al Kα monochromator ($h\nu$ = 1486.6 eV, power 600 W) as the X-ray source.

2.2.6. Thermogravimetric analysis

Thermogravimetric analysis (TGA) was used to analyze the thermal stability of compounds by a SHIMADZU mod, the TGA-50H system under an airflow (50 mL/min) and treated 3 times for each sample. The TGA instrument was run from the room temperature to 950 °C with a heating rate of 20 °C/min.

2.2.7. N_2 adsorption analysis and surface area calculations

Before measuring the gas sorption, the 100 mg of BioMOF, Fe-BioMOF and 5FU-BioMOF were activated through degassing under vacuum for 8 h at 130 °C. Conventional adsorption isotherm data were collected with Micromeritics Tristar 3000 volumetric instrument under the continuous adsorption conditions. The total specific surface areas for the N_2 isotherms at 77 K were calculated by Brunauer-Emmet-Teller (BET) and Langmuir analyses.

2.2.8. Adsorption and release of NO

For the adsorption and release studies of NO gas, a stainless steel 20-cm chromatographic column (with 0.4 cm internal diameter) was used to contain 100 mg of the samples (BioMOF, Fe-BioMOF and their related *in situ* synthesized fabric). The column of samples was activated under 20 ml/min flow of pure He gas at 130 °C overnight at Bruker Varian 450-GC Gas chromatographer. The gas mixture (Ar:NO 4:1) was prepared *via* mass flow controllers and passed through the activated samples for 5 min. The adsorption of NO was measured by Omnistar™ PFEIFFER Mass Spectrometer Gas Analysis System at 25 °C for gas peaks at *m/z* 30 (NO), 40 (Ar) and 4 (He). Since Gas Chromatography-Mass Spectroscopy (GC–MS) cannot detect the release behavior of samples, the constant Ar: humid mixture with 20 ml/min flow was passed through the sample column and the NO release behavior was studied by measuring color changing of modified Griess reagent aqueous solution according to the technical bulletin (Sigma-Aldrich). The absorbance peak was detected at 540 nm until 72 h by UV1800-Shimadzu UV–visible spectrophotometer.

2.2.9. Release behavior of 5FU

The 5FU encapsulation efficiency % was calculated according to Eq. (1) through detecting the free drug in the remained solution after washing 5FU-BioMOF. Indeed, the concentration of free 5FU was calculated by standard curve between absorbance and concentration at the maximum absorbance peak of 5FU at 264 nm (Fig. 3Sb). Moreover, in order to measure the loading capacity %, 20 mg of the 5FU-BioMOF was added to the water solution for seven days. After that, the releasing of 5FU was measured by UV1800-Shimadzu UV–visible spectrophotometer and 5FU loading capacity was calculated according to Eq. (2).

$$\text{5FU encapsulation efficiency\%} = (\text{total weight of drug} - \text{weight of drug in solution}) / \text{total weight of drug} \times 100 \quad (1)$$

$$\text{5FU loading capacity\%} = \text{weight of drug in 5FU} - \text{BioMOF} / \text{weight of 5FU} - \text{BioMOF taken} \times 100 \quad (2)$$

In order to evaluate 5FU release behaviors, 20 mg of 5FU-BioMOF was added to 2.0 mL of PBS (pH 7.4) at 37 °C. The 50 µl of this suspension was collected with 950 µl of PBS at each time and UV–Vis absorbance peak at 264 nm was measured to calculate the percentage of released 5FU according to Eq. (3); the 50 µl sample was returned to the mother release media.

$$\text{Release percentage (\%)} = \text{the amount of released 5FU at each time} / \text{the total amount of loaded 5FU} \times 100 \quad (3)$$

2.2.10. Kinetic analysis of release data

Data from release studies were fitted into the various mathematical drug release models (Table S1) by DDSolver free software to conclude the best model that refers to the kinetics of the drug release. Although every model was fitted to the total drug release data, for Korsmeyer-Peppas and Weibull models, only until 60% of data were fitted.

2.2.11. Antibacterial effect

The antibacterial activities of BioMOF and 5FU-BioMOF and their *in situ* synthesized on fabrics were tested against Gram-negative bacteria, *Escherichia coli* (*E. coli*) and the Gram-positive bacteria, *Staphylococcus aureus* (*S. aureus*), were cultured in Tryptic Soy Broth (TSB) medium at 37 °C for 24 h. Then, these grown bacteria were diluted to achieve a cell density of approximately 5×10^5 cells/ml. 50 µl of these media were added to soft agar (overlayer) tubes and kept in an over fusion at 50 °C. After that, the contents of the tubes were mixed gently and poured onto Trypticase Soy Agar (TSA) plates. The samples were deposited and incubated on each plate at 37 °C for 24 h.

2.2.12. In vitro cytotoxicity studies

In order to study cell viability, B16F10 (mouse melanoma) as the skin cancer cell line was used. The B16F10 cells were seeded onto 24-well plates at the density of 1×10^5 cells per well. The cell suspension was added into 24-well plates to preculture for 24 h by incubation at 37 °C in 5% CO_2 in Dulbecco's Modified Eagle Media (DMEM), 2 mM Glutamine and 10% Fetal Bovine Serum. The grown cells were treated with fresh medium containing the BioMOF, 5FU-BioMOF, BioMOF-Fa, 5FU-BioMOF-Fa in each well. For each sample, to prove the performance of 5FU-BioMOF and 5FU-BioMOF-Fa, free 5FU and 5FU-Fa were prepared at the same concentration of 5FU. The cytotoxicity test was carried out in triplicates after 24 h incubation. In order to analyze the viability of cell line, flow cytometry test was performed as mentioned below.

In order to flow cytometry study, the FACSCanto II analyzer was used and the result was evaluated with FACSDiva software. Each test contained within the measurements of around 10,000 cells. The treated cells were entirely washed with sterile PBS. Following, 1 mL of the cell suspension was moved to a fluorescence-activated cell sorting (FACS) tube and gently mixed with 5 µL annexin V-FITC (1 mg/mL) and 5 µL propidium iodide (PI) (2.5 mg/mL). The tubes were gradually mixed using a vortex mixer and incubated for 15 min at the ambient temperature in the dark. After adding Binding buffer (400 µL) to the FACS

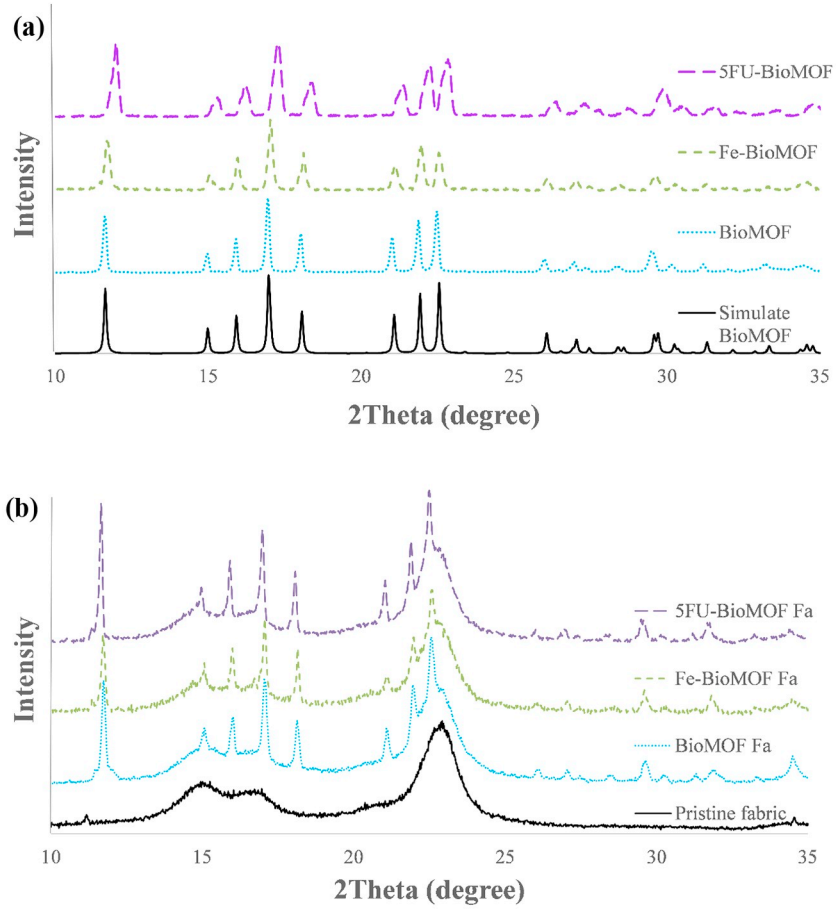

Fig. 2. XRPD patterns of simulate BioMOF, as synthesized BioMOF, Fe-BioMOF, 5FU-BioMOF (a), and pristine cotton fabric, BioMOF-Fa, Fe-BioMOF-Fa and 5FU-BioMOF-Fa (b).

tube, the tubes were set by a FACS analyzer for 1 h.

3. Results and discussions

3.1. BioMOF formation and application on cotton fabric

The target zinc glutamate BioMOF was formed according to the literature method [12]. By increasing the alkalinity, the carboxylate groups of the glutamate ligand become available for Zn coordination binding. The XRPD analysis evidences the formation of a pure crystalline phase of material (Fig. 2a). FTIR-ATR, XPS and TGA analyses further verified the formation of the desired material. Noteworthy, the Fe^{II} and 5FU doped BioMOF, Fe-BioMOF and 5FU-BioMOF remain isostructural to the parent BioMOF as confirmed from XRPD studies (Fig. 2a). Noteworthy, the XRPD pattern of the 5FU-BioMOF exhibit peak broadening as well as small shifts in the peak positions compared to the parent BioMOF XRPD pattern. This results point to the structural stress related to the actual incorporation of 5FU in the BioMOF framework and/or the pore structure [21].

The XRPD pattern of the treated cotton fabric is in agreement with the actual incorporation of the BioMOF particles on the cotton fabric (Fig. 2b). In these patterns, the peaks at 2θ 15.1°, 16.6° and 22.9° values correspond to the crystalline structure of pristine cotton fabric [22]. Based on the results of XRPD measurements, it can be concluded that BioMOF is deposited on the cotton fabric through *in situ* synthesis. In which, pretreatment of the cotton fabric with OH^- firstly formed the partial negative charge on the surface of cellulosic structure facilitating Zn^{2+} ions anchoring which is followed by BioMOF growth in the fabric fibers (Scheme 1). Therefore, cotton fabric behaves as a soft template for the controlled nucleation and growth of BioMOF nanostructure. A related behavior is also observed for the Fe^{II} and 5FU doped Fe-BioMOF and 5FU-BioMOF materials. This observation is in good accordance with the results by previous studies of the formation of nanostructures through *in situ* synthesis on cotton fabric [22,23].

3.2. FTIR-attenuated total reflectance (FTIR-ATR)

FTIR-ATR was used to further confirm the formation of BioMOF from zinc and glutamate in the presence of alkali media. The hydroxyl, amine and carboxyl groups of zinc glutamate BioMOF shift to 3170, 3324 and 1597, 1553 cm^{-1} vibrational band compared to the glutamic acid alone (Fig. 3a). Furthermore, the FTIR-ATR analysis showed that there is no significant difference in the peak position of the functional group between the BioMOF and one-pot synthesis of Fe^{II} doped Fe-BioMOF (Fig. 3a).

In the case of 5FU-BioMOF, the FTIR-ATR spectra confirm the presence of functional groups of 5FU (Fig. 3b). The absorption bands at 1180 cm^{-1}, 1245 cm^{-1}, 1650 cm^{-1} and 1720 cm^{-1} have been assigned to the stretching mode of C—N, C—F, C═C and C═O in this spectra, respectively [24–26]. The presence of these functional groups with insignificant shifting in the peaks' position exhibits that 5FU is encapsulated in 5FU-BioMOF with only hydrogen bonding or coordination reactions on the zinc side of BioMOF.

The presence of functional groups of BioMOF on the cotton fabric verifies the *in situ* synthesis of BioMOF on the cotton fabric is a powerful method to modify the cotton fabrics (Fig. 3c). The effect of 5FU on the cotton fabric was determined by treating with the same amount of 5FU on cotton fabric according to *in situ* synthesis 5FU-BioMOF-Fa

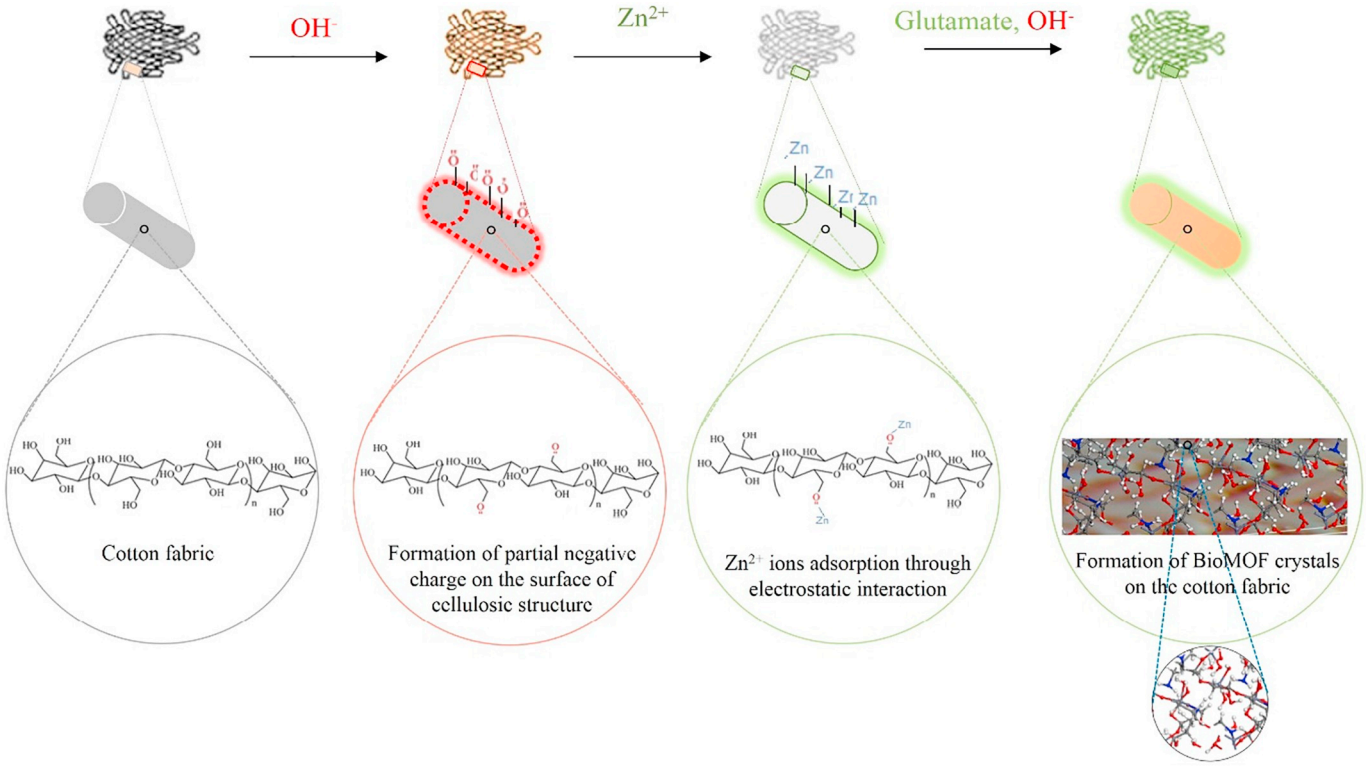

Scheme 1. Schematic of *In situ* synthesis of the BioMOF on cotton fabric.

preparation method. The FTIR-ATR, TGA and XPS analyses showed that there is no difference between 5FU-Fa and pristine cotton fabric (Fig. S1a). By careful and reasonable studies, we can conclude that there is no interaction and adsorption between 5FU and cotton fabric. However, the physical adsorption on the surface of cotton fabric cannot be ignored. Cell toxicity was performed for comparing the effects of 5FU on cotton fabric that will be discussed in the following part (3.12).

3.3. Morphology and size study

The FESEM images showed that several one-dimensional zinc glutamate tetragonal prisms formed the flower-like morphology for BioMOF with the conic apex (Fig. 4). Fig. 4b demonstrated that the radial pyramid-like rods were spread from the center to the flower surface of BioMOF.

The FESEM images of Fe-BioMOF and 5FU-BioMOF evidence that the morphology of BioMOF remains intact after taking Fe or 5FU (Fig. 4c,d). The EDX analysis showed that the presence of iron on Fe-BioMOF sample (Fig. 4e). The iron signal was detailed in EDX analysis for Fe-BioMOF endorsing the presence of Fe on Fe-BioMOF.

The FESEM image study sets out to determine the dispersing and uniform properties of BioMOF nanoparticles on the cotton fabric (Fig. 5). The most interesting finding was that *in situ* synthesis of BioMOF-Fa alters the morphology and size of BioMOF particles from flower-like with micro size rods to round-like with 101 ± 59 nm size. These results further support the idea that cellulosic fibers control the morphology and size of particles through *in situ* synthesis method [22,23]. Based on the EDX results, it is observed that *in situ* synthesis of BioMOF-Fa deposited a large amount of zinc compound compared to the pristine cotton fabric (Fig. 5d).

3.4. Diffuse reflectance UVis-NIR spectrophotometer

Fig. 6 shows the plots of diffuse reflectance UV-VIS-NIR spectrophotometer as a function to demonstrate the presence of Fe^{II} in Fe-BioMOF. What we know about the Tanabe-Sugano diagram of the electronic states for a d^6 ion in both high field (low spin) and low field (high spin) situations of Fe^{II}, that the ground state exists at $^5T_2$. Therefore, there is only one allowed transition: $^5T_2 \rightarrow {}^5E$ (the spin multiplicity cannot change) since the type of ligands (H_2O and COO^-) involved in Fe-BioMOF structure cannot create high crystal fields (Fig. S2). Consequently, the Fe^{II} octahedral peak showed a broad and weak peak around 900–1100 nm in Fig. 6.

3.5. XPS studies

The elemental analysis and oxidation state of the elements present in the samples have been analyzed by XPS (Fig. 7). The XPS analysis of BioMOF illustrates that this structure is composed of Zn, N, O, and C, and negligible peaks of Na and Cl elements as the impurity (Fig. 7a). The high-resolution scan of the Fe-BioMOF spectra shows there are binding energies of the Fe^{II} 2p3/2 and 2p1/2 at 710.0 eV and 724.6 eV, respectively. Another important finding was that the symmetric peak of zinc at 1020.33 and 1043.41 eV in this sample remained intact after loading Fe^{II}. Recent evidence and XRPD pattern of Fe-BioMOF suggest the idea of Fe^{II} will be replacing Zn^{II} in an isomorphous way, which means Fe^{II} easily accommodates in the octahedral environment of Zn^{II} without any changes in the crystallinity and phase purity of BioMOF structure.

The binding energy spectra of the 5FU-BioMOF and 5FU are shown in Fig. 7a. The F 1s peak at 686 eV, in agreement with the peak area of the pure 5FU spectrum, declares the one-pot synthesis method is efficient for loading 5FU on the BioMOF. As seen from Fig. 7a, the peaks of Zn 2p3/2 and 2p1/2 in BioMOF spectra were increased from 1020.33 eV and 1043.41 eV to 1020.52 eV and 1043.51 eV in 5FU-BioMOF, respectively [27]. In-depth, 5FU could form weak coordination bonds with Zn^{2+} ions at the first step [28]. By adding organic ligand as glutamate, the zinc ions are taken apart from 5FU molecules and consequently coordinate with glutamate to form the stable BioMOF networks.

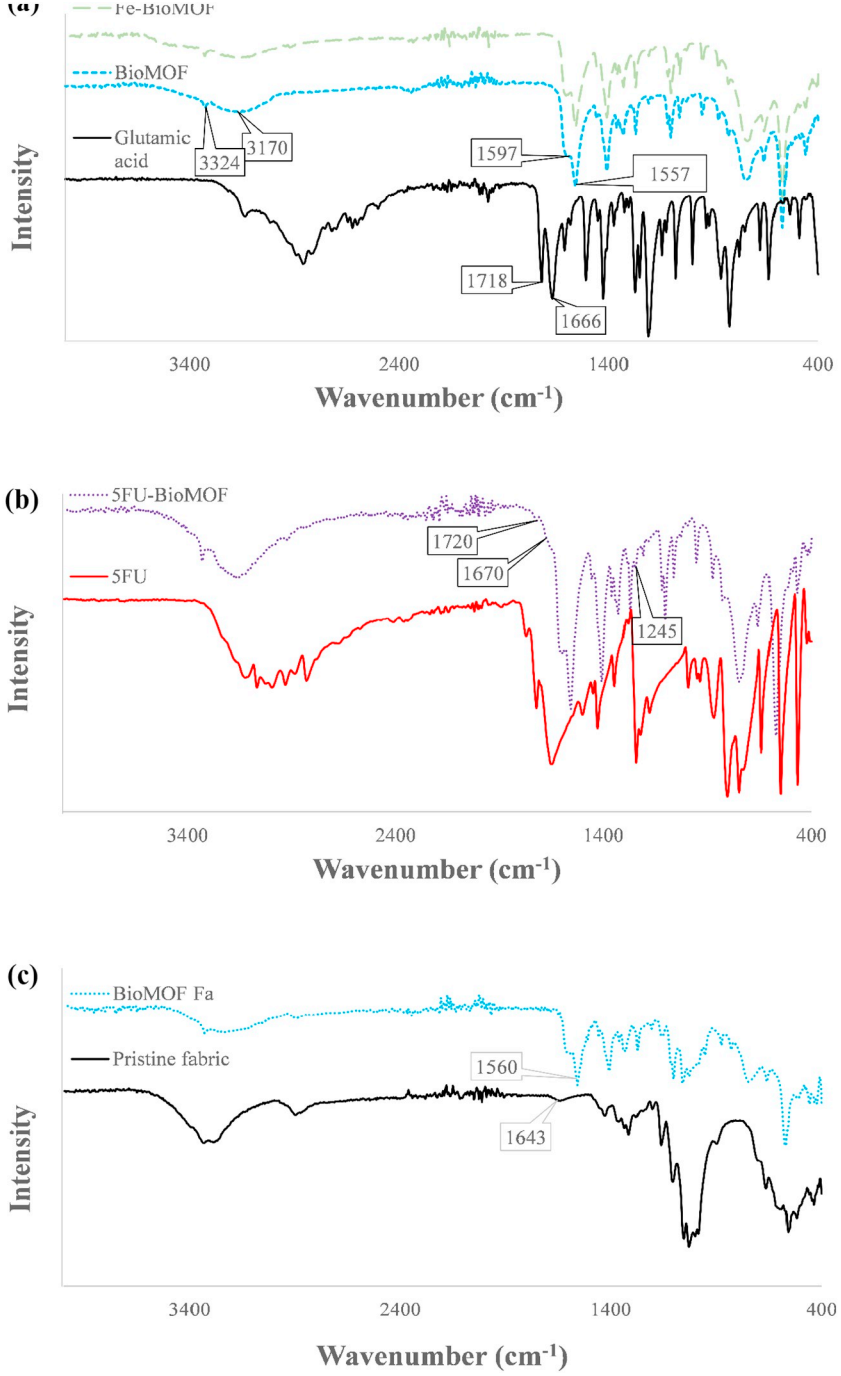

Fig. 3. FTIR-ATR analyses of Glutamic acid, BioMOF and Fe-BioMOF (a), 5FU, 5FU-BioMOF (b) and pristine fabric, BioMOF-Fa (c).

The signals of Zn 2p, C 1s, O 1s, and N 1s were detected in XPS spectra of the *in situ* synthesis BioMOF-Fa (Fig. 7b). Moreover, Fe 2p and F 1s were detected for *in situ* synthesis of Fe-BioMOF-Fa and 5FU-BioMOF-Fa. Nevertheless, there is no peak of F for 5FU-Fa, which means that the cotton fabric could not absorb the high amount of 5FU.

3.6. Thermogravimetric analysis

The variation in TGA spectra of BioMOF and Fe-BioMOF reflect the differences between them in weight loss above 620 °C (Fig. 8a). The weight loss below 620 °C, with respect to the reference samples (5FU and BioMOF), is attributed to the 5FU occupation in the pore space (or the framework) of the BioMOF (Fig. 8b). By mass loss in the result of thermal degradation, the amounts of Fe and 5FU in their powder samples were measured around 3.17 ± 1.4% and 1.69 ± 1.2% (w/w) respectively, consistent with FTIR-ATR, XPS, and loading capacity observation (Table S5). Likewise, the TGA analysis proved that the BioMOF was simply *in situ* synthesized on the cotton fabric. Also, the mass loss of the thermal degradation showed that iron and 5FU were straightforwardly loaded and deposited on the Fe-BioMOF and the 5FU-BioMOF, respectively (Fig. 8b). In the case of *in situ* synthesis of BioMOF-Fa, a subsisting powder is stable above 600 °C, which is related to zinc oxide. According to the molecular weight of BioMOF, this amount only showed 33.01% of the BioMOF mass. Therefore, the amount of *in situ* synthesized BioMOF was 13.96% of the treated cotton fabric weight, which is near to add-on percentage (13.25%) found according to eq. S1 (Table S3),

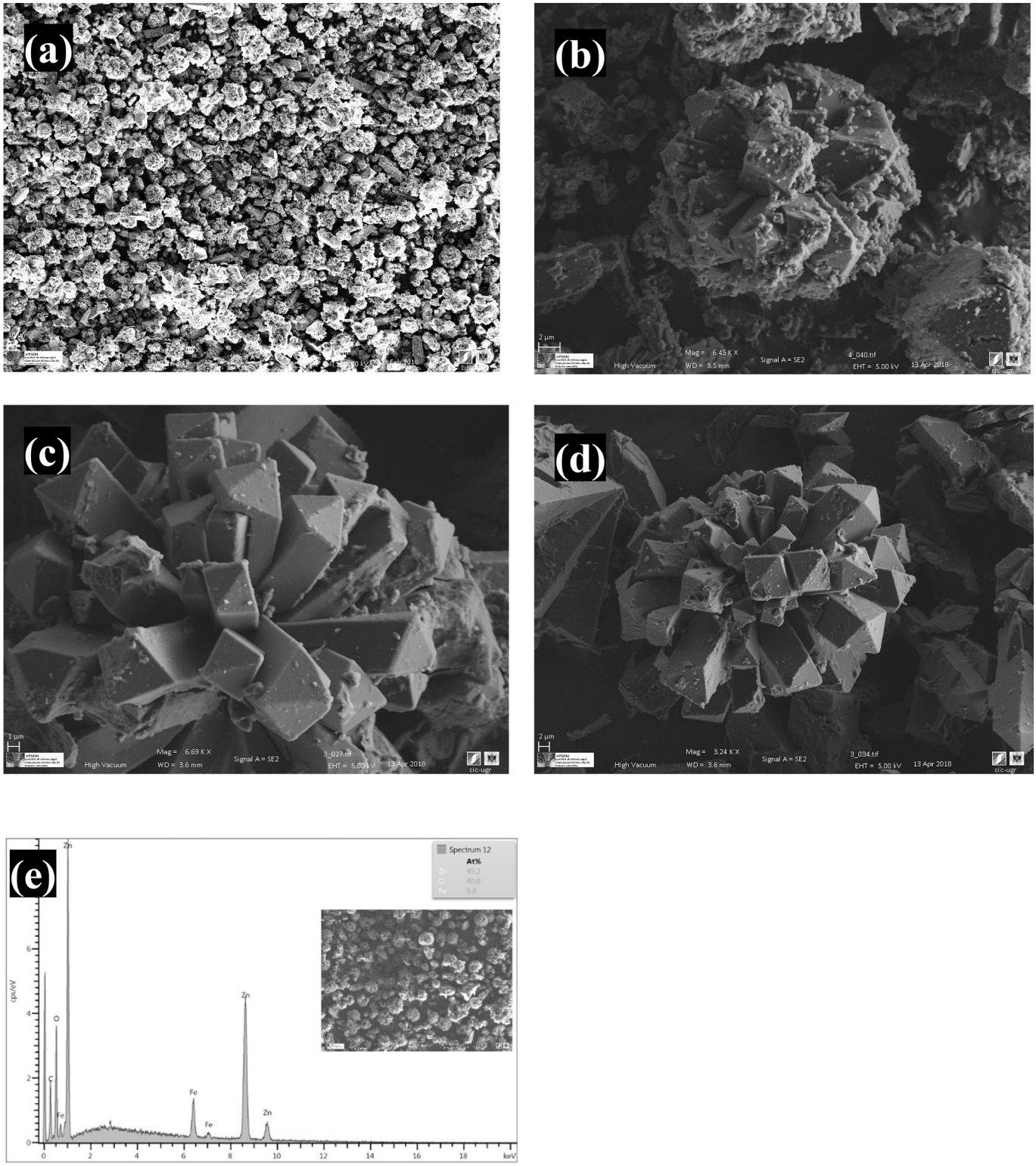

Fig. 4. FESEM images of BioMOF (a, b), Fe-BioMOF (c), 5FU-BioMOF (d) EDX image of Fe-BioMOF (e).

3.7. N_2 adsorption measurements

The surface area of the BioMOF significantly increases by the modification of structure with iron about 80% while the surface area of 5FU-BioMOF decreases about 22% upon loading 5FU (Table S4). However, the BioMOF pore size almost remains intact after loading Fe and 5FU, the actual pore volume changes about +130% and −27% due to load Fe as a defect and encapsulation of 5FU, respectively.

3.8. Release behavior of NO

In a first step, we studied the incorporation of NO in the BioMOF samples. In view of the poor performance of the pristine material, we decided to incorporate Fe^{II} active centers in the framework by doping

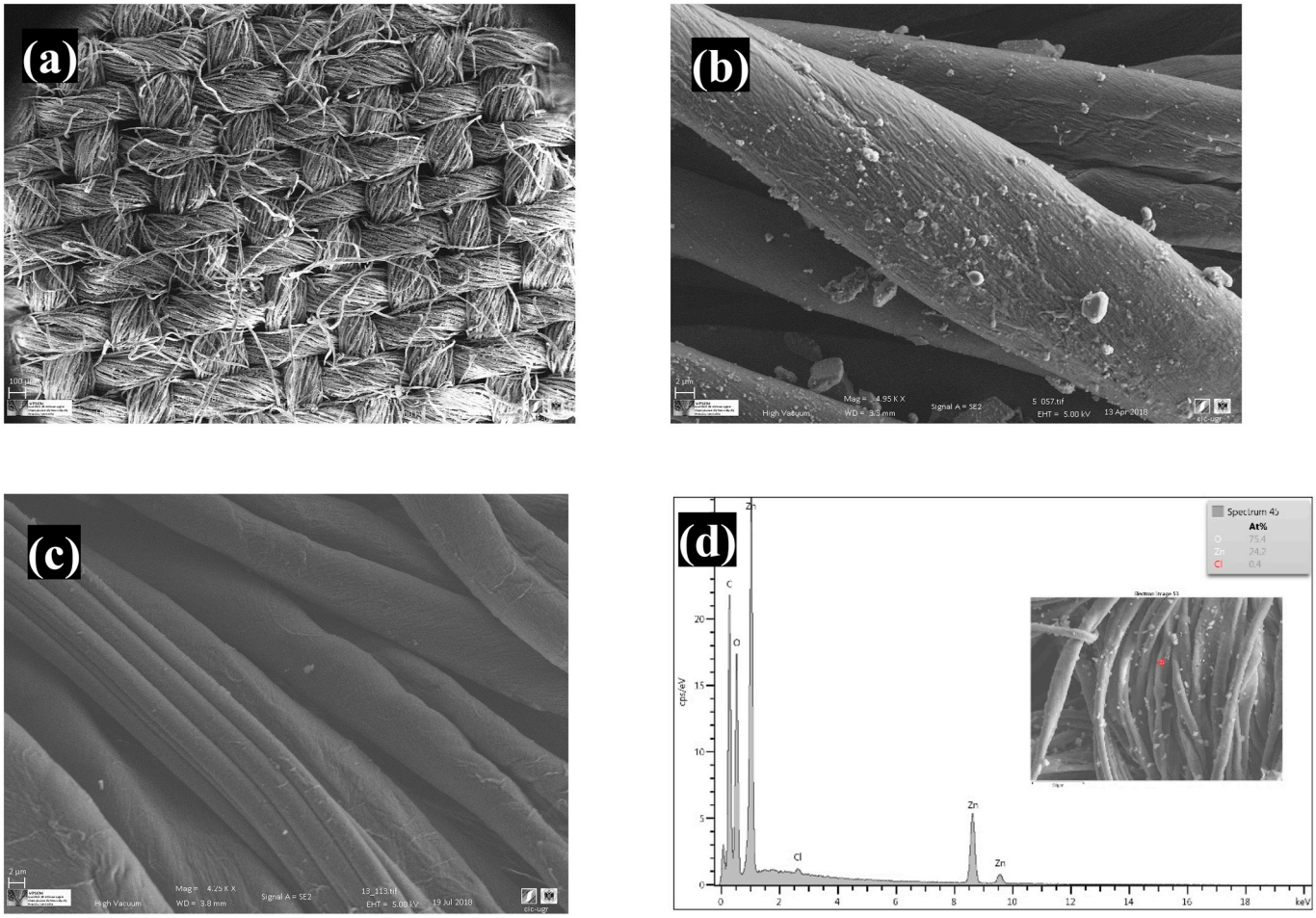

Fig. 5. FESEM images of BioMOF-Fa (a, b), pristine-Fa (c), EDX image of BioMOF-Fa (d).

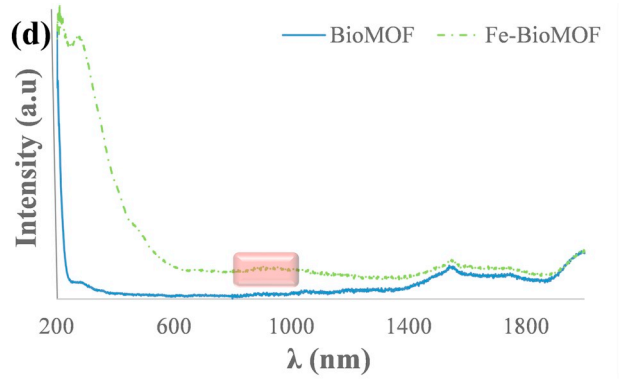

Fig. 6. Diffuse reflectance UV-VIS-NIR spectrophotometer of Fe^{II} in Fe-BioMOF.

the material to yield Fe-BioMOF. The results agree with a significant enhancement of NO adsorption upon Fe incorporation according to NO breakthrough measurements. The prominent peak of NO adsorption on Fe-BioMOF can be clearly seen in the GC–MS spectra (Fig. S4).

In order to analyze the NO release of the samples, a set up employing GC–MS and UV–Visible spectrophotometer were used. NO release behavior of BioMOF and Fe-BioMOF and their *in situ* synthesized fabrics are shown in Fig. 9. The results demonstrate a larger quantity of NO release from Fe-BioMOF and the release graph did not reach a plateau even after 72 h of testing, while Horcajada et al. reported that NO was released from flexible MIL-88(Fe) MOFs over a short period of time (> 16 h) [18]. Indeed, loading of Fe^{II} on BioMOF sample combines the advantage of NO coordination with iron and zinc. As a result, it showed higher adsorption of NO and releasing at a longer time as previously reported [29]. Moreover, the Fe-BioMOF-Fa exhibited significant potential for controlling the release of NO (Fig. 9b). Taking into account that a controlled release of NO gas during a long time interval would be useful for the promotion of wound dressings, which is desirable for infection prevention.

3.9. Release behavior of 5FU

The drug encapsulation efficiency showed that only 85.16% of 5FU encapsulated on BioMOF through one-pot synthesis method. From the standpoint of the drug loading capacity, the BioMOF structure was relatively a close structure and could load around 1.17% of 5FU on the weight of BioMOF. The evidence points to the probability that the rate of release would be relatively slow when the drug released [30]. Although the free 5FU released in PBS media during 10 min (Fig. S3), the same amount of the drug in 5FU-BioMOF released after 72 h (Fig. 9c). The XRPD analysis exhibits that BioMOF crystalline structure was stable even after 24 h in PBS solution. However, the BioMOF was degraded in acidic solution during 1 h (Fig. S3). This phenomenon gives evidence that BioMOF could be degraded and the drug entirely released in acidic pH. It is of interest to note also that the tumor tissue has mild acidic conditions [25,31,32]. By a careful and comparative study, we propose that 5FU-BioMOF can be used as a smart drug delivery system against tumor cells and reduced toxicity to the healthy cells.

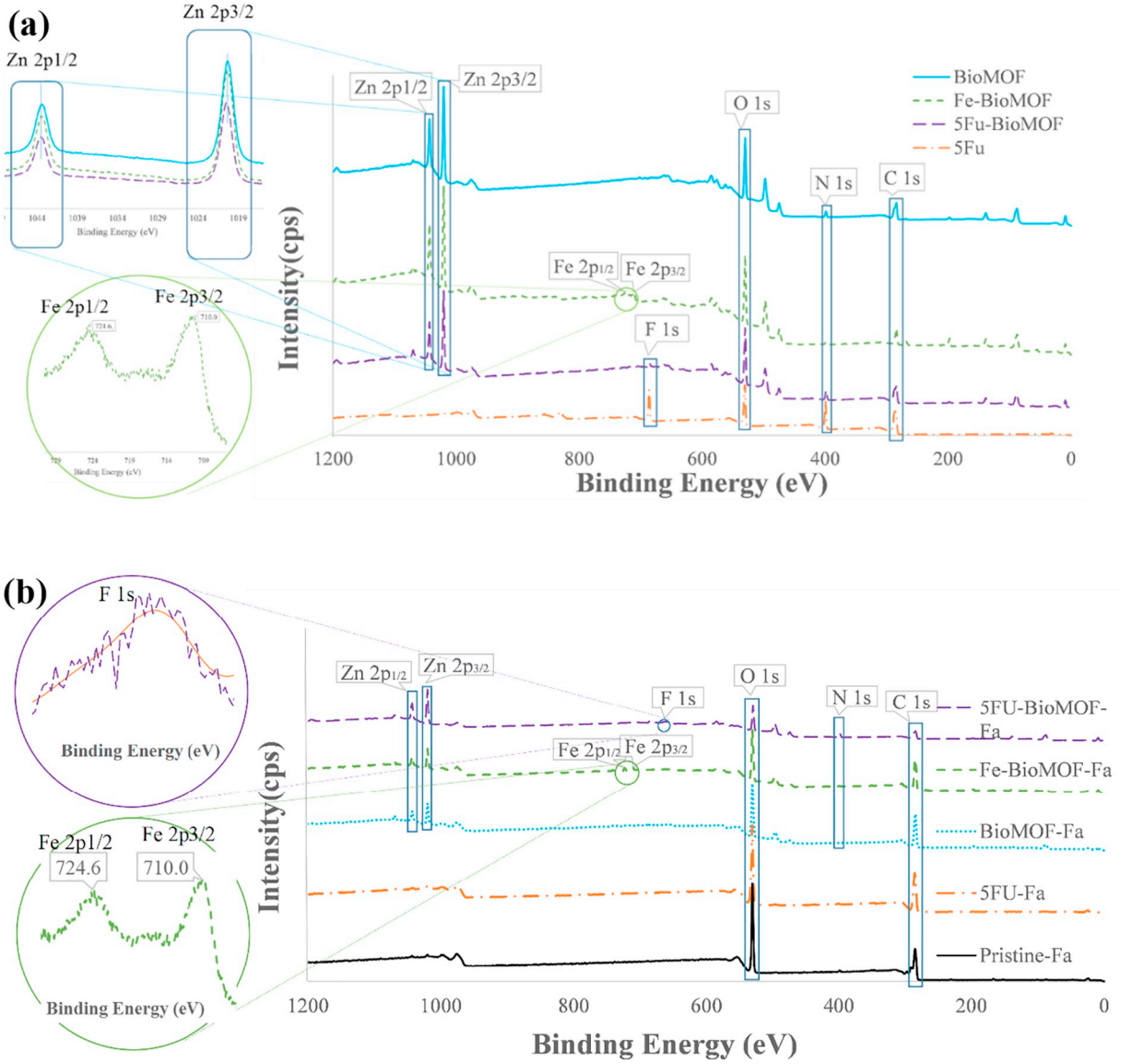

Fig. 7. XPS Analyses of sample powders with high resolution of Zn 2p, Fe 2p (a), and treated fabrics with high resolution of F 1s, Fe 2p (b).

3.10. Kinetic analysis of release data

The fitting of drug release data of 5FU-BioMOF by exact mathematical models declares the explanation and understanding of the release mechanisms involved in the drug delivery system, which is an important character to modulate the release behaviors of the sample in keeping with the specific therapeutic require [33].

The kinetic models, such as first-order, Higuchi, Hixson and Crowell, Baker and Lonsdale, Gompertz, Weibull and Korsmeyer-Peppas (Table S1), were applied on the drug release data of 5FU-BioMOF and the calculated respective coefficients were shown in Table S2. The well-matched model is the one which best fits the experimental data. The results showed that the Weibull model is fitted to 5FU-BioMOF with R^2 near one (0.9847).

However, the release mechanism can be considered such as (i) drug diffusion throughout the flexible pore structures, (ii) coordination or hydrogen bonding of 5FU with the powder network, and (iii) the erosion diffusion of the BioMOF matrix [24], in our case, the 5FU release mechanisms can be attributed to the combination of diffusion and interaction. In this way, the interaction of the drug with BioMOF matrix through the coordination of drug with zinc or hydrogen bonding cannot be ignored. Moreover, the releasing behavior of 5FU from 5FU-BioMOF was facing the diffusion mechanism rather than its self-erosion of 5FU-BioMOF matrix. Since the stability of 5FU-BioMOF in the PBS media during drug releases is considerable (Fig. S3c), which means the bulk degradation of the structure is trivial.

3.11. Antibacterial test

The antibacterial activity of the 5FU-BioMOF and 5FU-BioMOF-Fa were shown in Fig. 10. The bright area showed the region of inhibition zone area, which means the bacteria were not capable of growing. The inhibition zone diameter demonstrates that the 5FU leached out from 5FU-BioMOF and 5FU-BioMOF-Fa and killed the bacteria. The higher diameters of this area around the samples showed that the 5FU had a stronger influence on *Staphylococcus aureus (S. aureus)* than *Escherichia coli (E. coli)*. Both bacteria gram-negative and gram-positive were found alive on the pristine fabric as a control sample. The results showed that excellent antibacterial property on 5FU-BioMOF-Fa is due to load a sufficient amount of drug on BioMOF fabric through one-pot loading method.

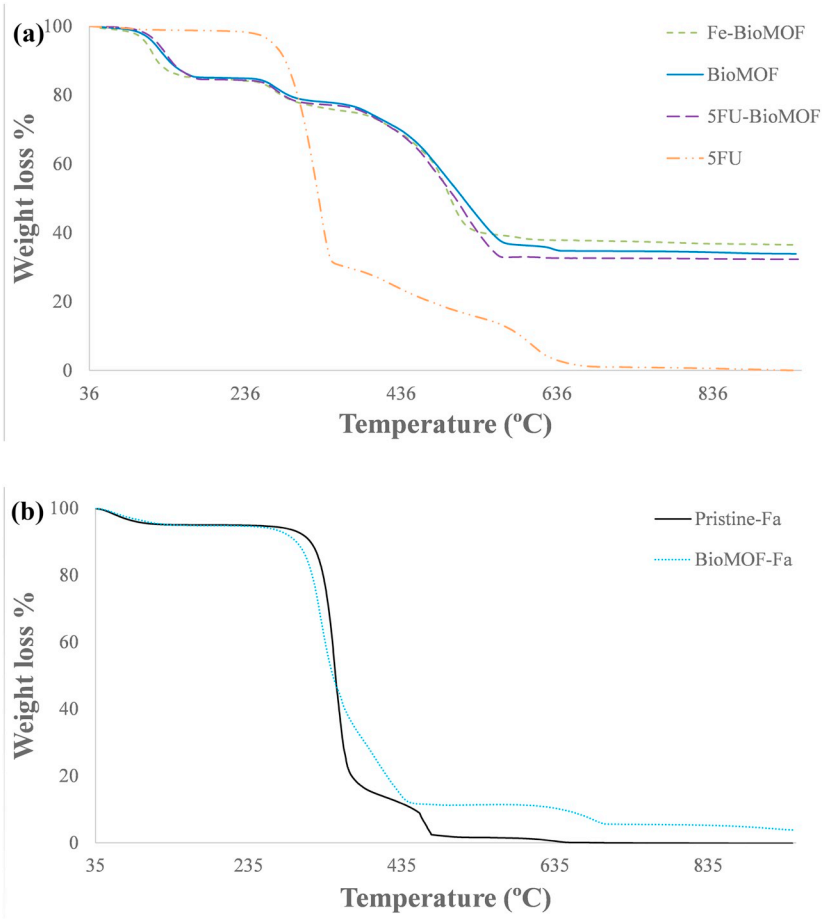

Fig. 8. TGA analyses of BioMOF, Fe-BioMOF, 5FU, 5FU-BioMOF (a) and pristine cotton fabric, BioMOF-Fa (b).

3.12. In vitro cytotoxicity studies

We selected flow cytometry test to analyses the cytotoxic of samples against B16F10 cells (Fig. 11). The results showed that the cell viability of BioMOF and pristine cotton fabric structures is around 90% during 24 h and indicating the excellent biocompatibility of these structures as their precursor [34].

The current work used 5FU at three different concentrations as a free drug to demonstrate the effectiveness of 5FU in cytotoxicity of melanoma treatment. 3 μg/ml free 5FU, as the same concentration of drug in 5FU-BioMOF, was applied to B16F10 skin cancer cells. Free 5FU is not efficient toxicity property due to the most probably the incapacity to reach the therapeutic doses at the selected skin cancer. Furthermore, associated systemic toxicity significantly confines their therapeutic index in which the owing course follows weak prognosis [32]. Since there is no significant cytotoxicity for the BioMOF and pristine fabric, higher cytotoxicity of 5FU-BioMOF and 5FU-BioMOF-Fa can be ascribed to the higher intracellular concentration and controlled release of the 5FU. Therefore, the drug delivery system for 5FU introduces the significant potential for improving the toxicity effect, is desirable in cancer chemotherapy due to diminishing drug dose and side effects.

The *in situ* synthesis and one-pot loading of 5FU-BioMOF on cotton fabric exhibited more cytotoxic effects over all the experimental samples. Moreover, there was a significant difference in cell viability of 5FU-BioMOF-Fa (27%) compared to 5FU-Fa (79%). Furthermore, 5FU-BioMOF-Fa confirms higher cytotoxicity comparing with 5FU-BioMOF due to the smaller size of nanocomposites through *in situ* synthesizing on the cotton fabric. The nanocomposites perhaps enter to fibroblast and disturb the natural metabolism of cancer cells. The dot plot of annexin V-FITC *versus* PI of samples is shown in Fig. S5.

However, this study provides novel method insight into the drug delivery in cancer therapy and wound healing for improving human healthcare against skin cancer and bacteria. We consider that this system should be further studied in other cancer cells, especially *in vivo* test, to approve the effectiveness with great insurance.

4. Conclusion

Thanks to the growth of the BioMOF field of technology and ability of its applications in textile wound dressing, this research emphasized on the *in situ* synthesis of BioMOF structure with safe raw materials and then used them as a bioactive molecule delivery system for cellulosic wound dressing. Therefore, we have succeeded in the *in situ* synthesis of Fe^{II} on BioMOF and *in situ* one-step encapsulation of 5FU in BioMOF by demonstrating the controlled release and skin cancer therapy. The chemical and structural evidence indicated that the flexible adsorption site inside the BioMOF structure provides the loading capacity for the metal and drug. Furthermore, the chemical and structural stability of BioMOF strongly depends on the pH; as a consequence, it offers the smart drug delivery system for releasing 5FU on the acidic pH of the tumor tissue. Moreover, since the cellulosic fabric control size of the particle through *in situ* synthesis method, we have successfully *in situ* synthesized nano BioMOF on the cotton fabric and also loading Fe^{II} and drug were prepared at one step of *in situ* synthesizing, even using bio-friendly and mild conditions. Therefore, the modification of flexible BioMOF with bioactive molecules and application on the cotton fabric provides significant antibacterial property and high toxicity for a skin cancer cell, it seems to have a bright future for the modification of cellulosic wound dressing by the BioMOF.

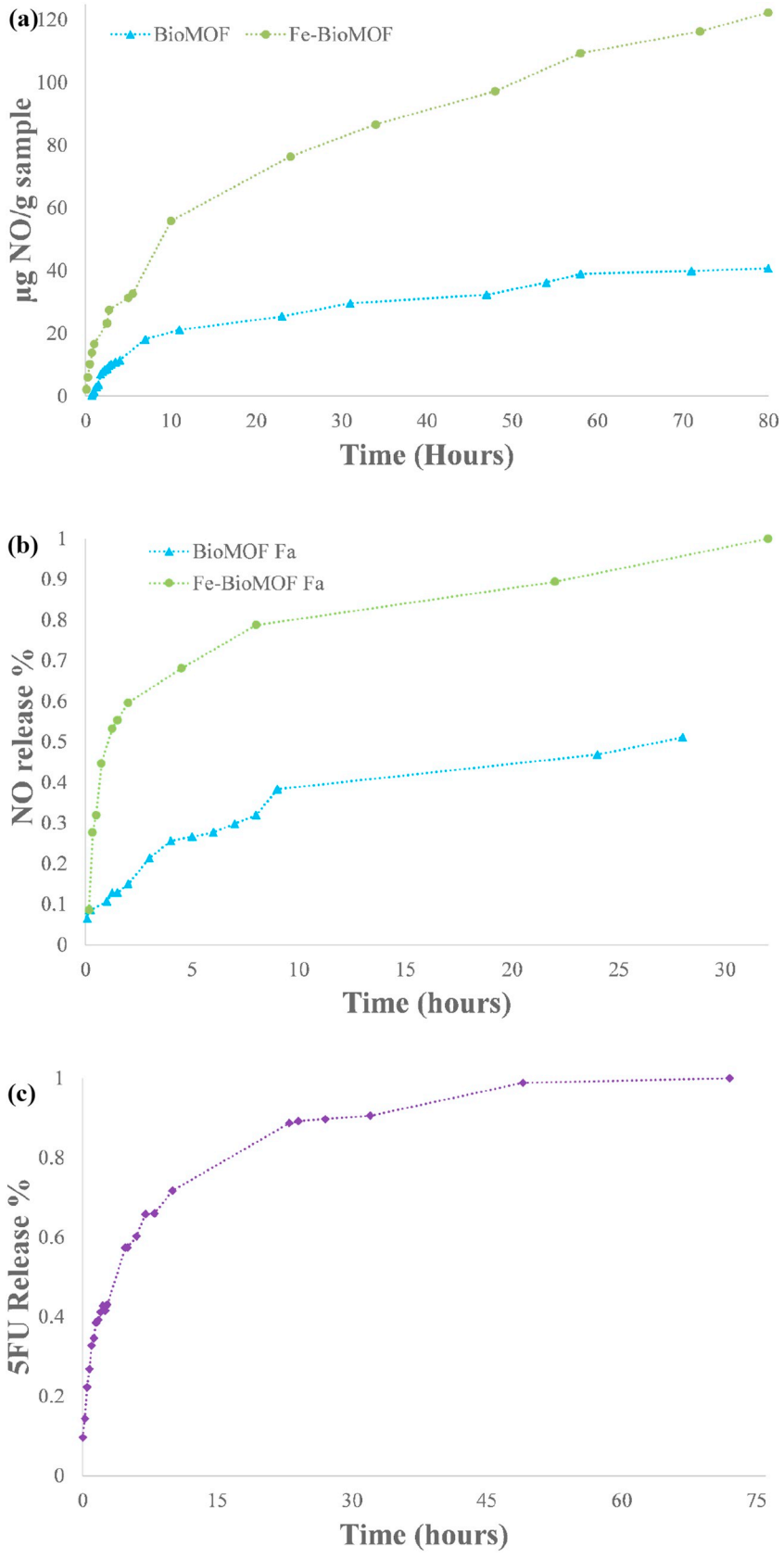

Fig. 9. NO release behavior of BioMOF and Fe-BioMOF (a), BioMOF-Fa and Fe-BioMOF-Fa through passing Ar:humid mixture (b) and 5FU release behavior of 5FU-BioMOF in PBS media (c).

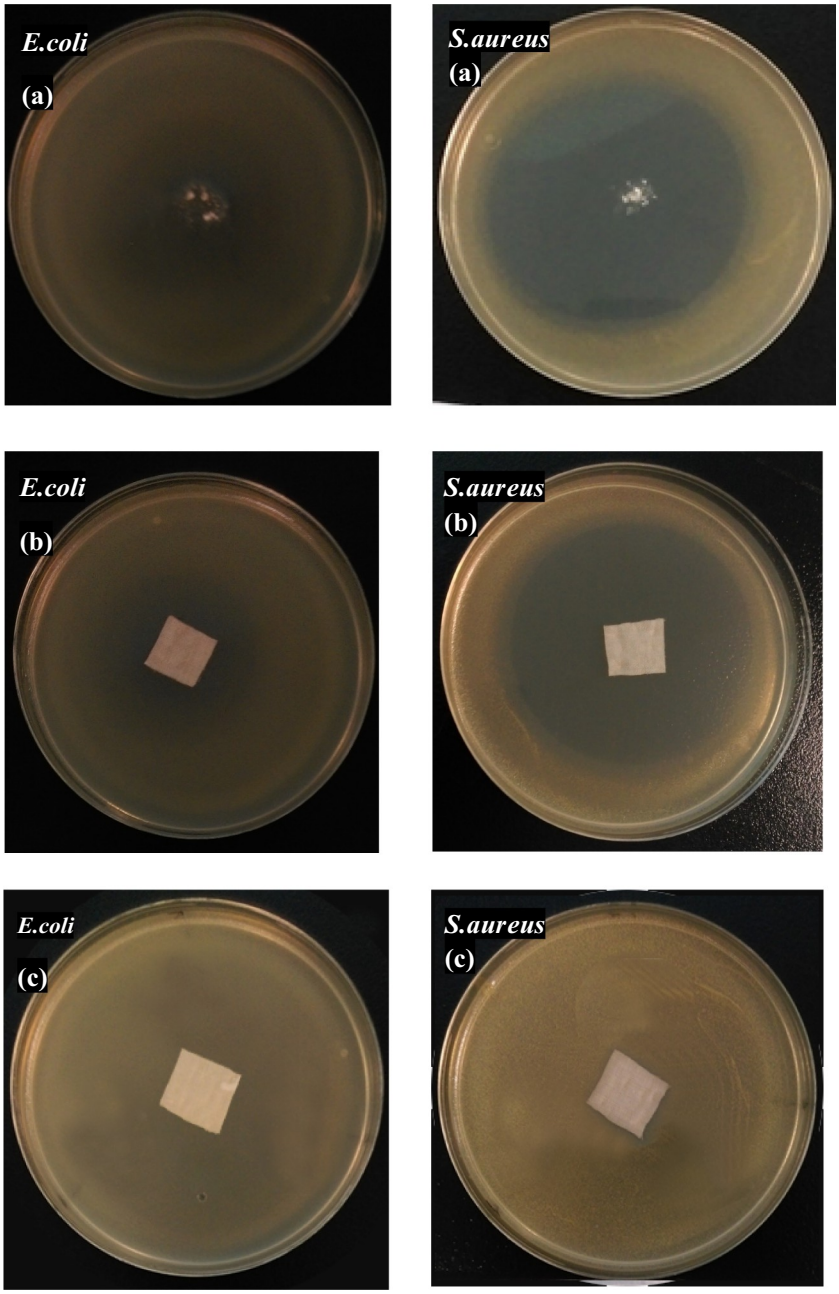

Fig. 10. Antibacterial activity of 5FU-BioMOF (a), 5FU-BioMOF-Fa (b), pristine-Fa (c) against *E.coli* and *S.aureus* bacteria.

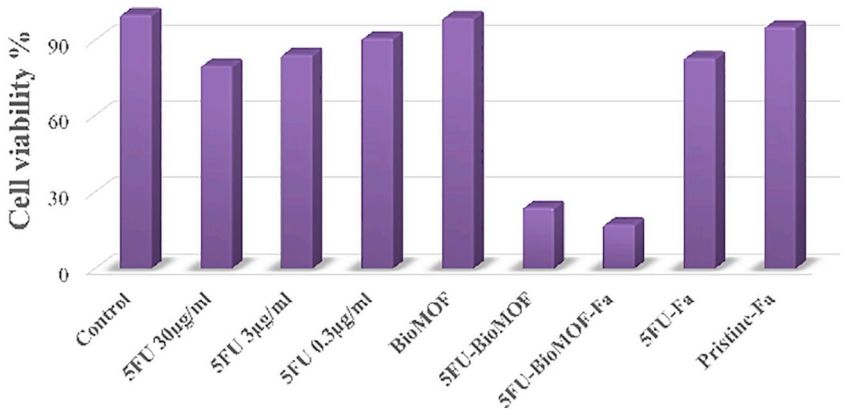

Fig. 11. Flow cytometry test against B16F10 Cell line.

Abbreviations

BioMOF	Zinc glutamate Bio Metal-Organic framework
5FU	5Flourouracil
NO	Nitric oxide
PBS	Dulbecco's Phosphate buffered saline
Fa	cotton fabric
S. aureus	*Staphylococcus aureus*
E. coli	*Escherichia coli*
XRPD	X-ray powder diffraction
FTIR-ATR	Fourier-Transform Infrared Spectroscopy-Attenuated Total Reflectance
FESEM	Field Emission Scanning Electron Microscopy (FESEM)
XPS	X-Ray Photoelectron Spectroscopy
TGA	Thermogravimetric Analysis
GC–MS	Gas Chromatography-Mass Spectroscopy
DMEM	Dulbecco's Modified Eagle Media
FACS	fluorescence-activated cell sorting

Appendix A. Supplementary data

Supplementary data to this article can be found online at https://doi.org/10.1016/j.jinorgbio.2019.110818.

References

[1] W. Zou, A. González, D. Jampaiah, R. Ramanathan, M. Taha, S. Walia, S. Sriram, M. Bhaskaran, J.M. Dominguez-Vera, V. Bansal, Skin color-specific and spectrally-selective naked-eye dosimetry of UVA, B and C radiations, Nat. Commun. 9 (2018) 3743, https://doi.org/10.1038/s41467-018-06273-3.

[2] H.D.M. Follmann, I. Messias, M.N. Queiroz, R.A. Araujo, A.F. Rubira, R. Silva, Designing hybrid materials with multifunctional interfaces for wound dressing, electrocatalysis, and chemical separation, J. Colloid Interface Sci. 533 (2019) 106–125, https://doi.org/10.1016/j.jcis.2018.08.007.

[3] S. Hashemikia, N. Hemmatinejad, E. Ahmadi, M. Montazer, Antibacterial and anti-inflammatory drug delivery properties on cotton fabric using betamethasone-loaded mesoporous silica particles stabilized with chitosan and silicone softener, Drug Deliv 23 (2016) 2946–2955, https://doi.org/10.3109/10717544.2015.1132795.

[4] E. Quartapelle Procopio, S. Rojas, N.M. Padial, S. Galli, N. Masciocchi, F. Linares, D. Miguel, J.E. Oltra, J.A.R. Navarro, E. Barea, Study of the incorporation and release of the non-conventional half-sandwich ruthenium(ii) metallodrug RAPTA-C on a robust MOF, Chem. Commun. 47 (2011) 11751–11753, https://doi.org/10.1039/c1cc14594k.

[5] W. Cai, J. Wang, C. Chu, W. Chen, C. Wu, G. Liu, Metal-organic framework-based stimuli-responsive systems for drug delivery, Adv. Sci. 6 (2019) 1801526, , https://doi.org/10.1002/advs.201801526.

[6] S. Rojas, I. Colinet, D. Cunha, T. Hidalgo, F. Salles, C. Serre, N. Guillou, P. Horcajada, Toward understanding drug incorporation and delivery from biocompatible metal–organic frameworks in view of cutaneous administration, ACS Omega 3 (2018) 2994–3003, https://doi.org/10.1021/acsomega.8b00185.

[7] X. Gao, Y. Wang, G. Ji, R. Cui, Z. Liu, One-pot synthesis of hierarchical-pore metal–organic frameworks for drug delivery and fluorescent imaging, CrystEngComm 20 (2018) 1087–1093, https://doi.org/10.1039/C7CE02053H.

[8] R. Monteagudo-Olivan, M.J. Cocero, J. Coronas, S. Rodríguez-Rojo, Supercritical CO2 encapsulation of bioactive molecules in carboxylate based MOFs, J. CO2 Util. 30 (2019) 38–47, https://doi.org/10.1016/j.jcou.2018.12.022.

[9] S. Rojas, F.J. Carmona, C.R. Maldonado, P. Horcajada, T. Hidalgo, C. Serre, J.A.R. Navarro, E. Barea, Nanoscaled zinc pyrazolate metal-organic frameworks as drug-delivery systems, Inorg. Chem. 55 (2016) 2650–2663, https://doi.org/10.1021/acs.inorgchem.6b00045.

[10] H. Cai, Y.-L. Huang, D. Li, Biological metal–organic frameworks: structures, host–guest chemistry and bio-applications, Coord. Chem. Rev. 378 (2019) 207–221, https://doi.org/10.1016/j.ccr.2017.12.003.

[11] P. Long, Q. Zhao, J. Dong, J. Li, Synthesis of metal-organic frameworks from the system metal/L-glutamic acid/TEA/H2O, J. Coord. Chem. 62 (2009) 1959–1963, https://doi.org/10.1080/00958970902737903.

[12] A.C. Kathalikkattil, R. Roshan, J. Tharun, R. Babu, G.-S. Jeong, D.-W. Kim, S.J. Cho, D.-W. Park, A sustainable protocol for the facile synthesis of zinc-glutamate MOF: an efficient catalyst for room temperature CO 2 fixation reactions under wet conditions, Chem. Commun. 52 (2016) 280–283, https://doi.org/10.1039/C5CC07781H.

[13] M.-X. Wu, Y.-W. Yang, Metal-organic framework (MOF)-based drug/cargo delivery and cancer therapy, Adv. Mater. 29 (2017) 1606134, , https://doi.org/10.1002/adma.201606134.

[14] S. Begum, Z. Hassan, S. Bräse, C. Wöll, M. Tsotsalas, Metal–organic framework-templated biomaterials: recent progress in synthesis, functionalization, and applications, Acc. Chem. Res. (2019), https://doi.org/10.1021/acs.accounts.9b00039 acs.accounts.9b00039.

[15] C.K. Brozek, J.T. Miller, S.A. Stoian, M. Dinca, NO disproportionation at a mononuclear site-isolated Fe2+ center in Fe2+-MOF-5, J. Am. Chem. Soc. 137 (2015) 7495–7501, https://doi.org/10.1021/jacs.5b03761.

[16] F. Kabirian, B. Ditkowski, A. Zamanian, M.F. Hoylaerts, M. Mozafari, R. Heying, Controlled NO-release from 3D-printed small-diameter vascular grafts prevents platelet activation and bacterial infectivity, ACS Biomater. Sci. Eng. (2019), https://doi.org/10.1021/acsbiomaterials.9b00220 acsbiomaterials.9b00220.

[17] E. Barea, C. Montoro, J.A.R. Navarro, Toxic gas removal – metal–organic frameworks for the capture and degradation of toxic gases and vapours, Chem. Soc. Rev. 43 (2014) 5419–5430, https://doi.org/10.1039/C3CS60475F.

[18] A.C. McKinlay, J.F. Eubank, S. Wuttke, B. Xiao, P.S. Wheatley, P. Bazin, J.-C. Lavalley, M. Daturi, A. Vimont, G. De Weireld, P. Horcajada, C. Serre, R.E. Morris, Nitric oxide adsorption and delivery in flexible MIL-88(Fe) metal–organic frameworks, Chem. Mater. 25 (2013) 1592–1599, https://doi.org/10.1021/cm304037x.

[19] Y.A. Workie, Sabrina, T. Imae, M.P. Krafft, Nitric oxide gas delivery by fluorinated poly(ethylene glycol)@graphene oxide carrier toward pharmacotherapeutics, ACS Biomater. Sci. Eng. 5 (2019) 2926–2934, https://doi.org/10.1021/acsbiomaterials.9b00474.

[20] R.R. Tuttle, H.N. Rubin, C.D. Rithner, R.G. Finke, M.M. Reynolds, Copper ion vs copper metal–organic framework catalyzed NO release from bioavailable S-nitrosoglutathione en route to biomedical applications: direct 1H NMR monitoring in water allowing identification of the distinct, true reaction stoichiometries and thio, J. Inorg. Biochem. 199 (2019) 110760, , https://doi.org/10.1016/j.jinorgbio.2019.110760.

[21] L. Bai, S.Z.F. Phua, W.Q. Lim, A. Jana, Z. Luo, H.P. Tham, L. Zhao, Q. Gao, Y. Zhao, Nanoscale covalent organic frameworks as smart carriers for drug delivery, Chem. Commun. 52 (2016) 4128–4131, https://doi.org/10.1039/C6CC00853D.

[22] S.A. Noorian, N. Hemmatinejad, A. Bashari, One-pot synthesis of Cu 2 O/ZnO nanoparticles at present of folic acid to improve UV-protective effect of cotton fabrics, Photochem. Photobiol. 91 (2015) 510–517, https://doi.org/10.1111/php.12420.

[23] R. Dastjerdi, S. Noorian, Polysiloxane features on different nanostructure geometries; nano-wires and nano-ribbons, Colloids Surfaces A Physicochem. Eng. Asp. 452 (2014) 25–31, https://doi.org/10.1016/j.colsurfa.2014.03.063.

[24] S. Yan, J. Zhu, Z. Wang, J. Yin, Y. Zheng, X. Chen, Layer-by-layer assembly of poly (l-glutamic acid)/chitosan microcapsules for high loading and sustained release of 5-fluorouracil, Eur. J. Pharm. Biopharm. 78 (2011) 336–345, https://doi.org/10.1016/j.ejpb.2010.12.031.

[25] C. Sun, C. Qin, X.-L. Wang, G.-S. Yang, K. Shao, Y.-Q. Lan, Z.-M. Su, P. Huang, C.-G. Wang, E.-B. Wang, Zeolitic imidazolate framework-8 as efficient pH-sensitive drug delivery vehicle, Dalt. Trans. 41 (2012) 6906, https://doi.org/10.1039/c2dt30357d.

[26] L. Huang, W. Sui, Y. Wang, Q. Jiao, Preparation of chitosan/chondroitin sulfate complex microcapsules and application in controlled release of 5-fluorouracil, Carbohydr. Polym. 80 (2010) 168–173, https://doi.org/10.1016/j.carbpol.2009.11.007.

[27] W. Liu, X. Li, Y. Wong, W. Zheng, Y. Zhang, W. Cao, T. Chen, Selenium nanoparticles as a carrier of 5-fluorouracil to achieve anticancer synergism, ACS Nano 6 (2012) 6578–6591, https://doi.org/10.1021/nn202452c.

[28] X. Chen, R. Tong, Z. Shi, B. Yang, H. Liu, S. Ding, X. Wang, Q. Lei, J. Wu, W. Fang, MOF nanoparticles with encapsulated autophagy inhibitor in controlled drug delivery system for antitumor, ACS Appl. Mater. Interfaces 10 (2018) 2328–2337, https://doi.org/10.1021/acsami.7b16522.

[29] J.G. Nguyen, K.K. Tanabe, S.M. Cohen, Postsynthetic diazeniumdiolate formation and NO release from MOFs, CrystEngComm 12 (2010) 2335, https://doi.org/10.1039/c000154f.

[30] L. Zhang, Y. Chen, R. Shi, T. Kang, G. Pang, B. Wang, Y. Zhao, X. Zeng, C. Zou, P. Wu, J. Li, Synthesis of hollow nanocages MOF-5 as drug delivery vehicle to solve the load-bearing problem of insoluble antitumor drug oleanolic acid (OA), Inorg. Chem. Commun. 96 (2018) 20–23, https://doi.org/10.1016/j.inoche.2018.07.029.

[31] X. Chen, Z. Shi, R. Tong, S. Ding, X. Wang, J. Wu, Q. Lei, W. Fang, Derivative of epigallocatechin-3-gallatea encapsulated in ZIF-8 with polyethylene glycol–folic acid modification for target and pH-responsive drug release in anticancer research, ACS Biomater. Sci. Eng. 4 (2018) 4183–4192, https://doi.org/10.1021/acsbiomaterials.8b00840.

[32] S. Kumari, A.K. Kondapi, Lactoferrin nanoparticle mediated targeted delivery of 5-fluorouracil for enhanced therapeutic efficacy, Int. J. Biol. Macromol. 95 (2017) 232–237, https://doi.org/10.1016/j.ijbiomac.2016.10.110.

[33] F.M. Carbinatto, A.D. de Castro, R.C. Evangelista, B.S.F. Cury, Insights into the swelling process and drug release mechanisms from cross-linked pectin/high amylose starch matrices, Asian J. Pharm. Sci. 9 (2014) 27–34, https://doi.org/10.1016/j.ajps.2013.12.002.

[34] R.J. Hickey, D.J. Modulevsky, C.M. Cuerrier, A.E. Pelling, Customizing the shape and microenvironment biochemistry of biocompatible macroscopic plant-derived cellulose scaffolds, ACS Biomater. Sci. Eng. 4 (2018) 3726–3736, https://doi.org/10.1021/acsbiomaterials.8b00178.